AIMS Mathematics, 9(1): 1939–1958.
DOI: 10.3934/math.2024096
Received: 24 September 2023
Revised: 22 November 2023
Accepted: 04 December 2023
Published: 18 December 2023

http://www.aimspress.com/journal/Math

Research article

An ACA-BM-SBM for 2D acoustic sensitivity analysis

Liyuan Lan[1], Zhiyuan Zhou[2], Hanqing Liu[1], Xing Wei[3] and Fajie Wang[1,*]

[1] National Engineering Research Center for Intelligent Electrical Vehicle Power System, College of Mechanical and Electrical Engineering, Qingdao University, Qingdao 266071, China
[2] Viterbi School of Engineering, University of Southern California, Los Angeles, CA 90015, USA
[3] College of Civil Engineering and Architecture, East China Jiaotong University, Nanchang 330013, China

* **Correspondence:** Email: wfj1218@126.com.

Abstract: In this paper, we present a novel computational approach (named ACA-BM-SBM) for the calculation of 2D acoustic sensitivity by combining the Burton-Miller-type singular boundary method (BM-SBM) with the adaptive cross-approximation (ACA) algorithm. The BM-SBM circumvents the source singularities of the fundamental solutions by introducing the origin intensity factors, and it eliminates the fictitious frequency problem in external acoustic fields by introducing the Burton-Miller formula. As a semi-analysis meshless method, the BM-SBM can accurately solve the external acoustic problem governed by the Helmholtz equation. Nevertheless, the computational inefficiency introduced by the dense coefficient matrix renders this method suboptimal, particularly for large-scale simulations. As the number of nodes increases, the computation time and store memory increase dramatically. ACA is a purely algebraic method based on hierarchical matrices which can be used to partition the coefficient matrix step by step. By employing ACA, the BM-SBM can be effectively accelerated, and this results in less computation time, as well as fewer memory requirements. Numerical experiments, including Dirichlet and Neumann boundary conditions, illustrate that the proposed approach is an accurate, efficient and fast numerical method for acoustic sensitivity analysis.

Keywords: Burton-Miller-type singular boundary method; adaptive cross-approximation; acoustic sensitivity analysis; fast algorithm
Mathematics Subject Classification: 65N35, 68W99, 76M99

1. Introduction

Acoustic sensitivity analysis reveals the relationship between acoustic physical values and design variables, and it is a crucial part of acoustic optimization design [1–5]. In the last few decades, various numerical simulation methods have played a significant role in solving acoustic sensitivity analysis. The finite element method (FEM) [6–8], the boundary element method (BEM) [9–11] and some meshless methods [12–15] are currently the mainstream numerical tools. Among them, the FEM requires complicated mesh division, which results in a high calculation cost and long pre-processing time. In particular, the FEM must artificially setup a finite domain with an absorbing layer when applied to an external acoustic field. The BEM is widely applied in the field of acoustic radiation and scattering since its basis function satisfies the governing equation of acoustic problems and the Sommerfeld condition at infinity. In addition, the BEM reduces the dimension of the computational problem because only the boundary of the computational domain is required to be discretized. However, the BEM has to solve the singular integrals, which is a cumbersome and time-consuming task.

To avoid the disadvantages of the FEM and BEM, many scholars have proposed various meshless methods, such as the generalized finite difference method [16,17], the element-free Galerkin method [18,19], the meshless local Petrov-Galerkin approach [20,21], the method of fundamental solutions (MFS) [22,23], the boundary knot method [24,25] and the singular boundary method (SBM) [26,27]. Among the above methods, the MFS adopts the same kernel function as the BEM, and therefore is only required to discretize the boundary of the computational domain. Meanwhile, the MFS requires selection of the fictitious boundary outside of the computational domain to eliminate the source singularity. However, as the precise arrangement of the fictitious boundary plays a crucial role in ensuring the accuracy of the MFS, the development of an effective method for constructing the fictitious boundary in irregular and complex geometries has become an urgent and pivotal issue to address in current research.

The SBM is a semi-analysis and boundary-type meshless method proposed by Chen in 2009 [28]. This method discards the fictitious boundary in the MFS by introducing the origin intensity factors (OIFs) [29]. In addition, the method inherits the advantages of the BEM and MFS, and it is simple and accurate due to the use of a fundamental solution, especially for acoustic scattering or radiation problems. Like the BEM, the SBM may encounter the issue of fictitious eigenfrequencies when solving external acoustic field problems. In this regard, Fu et al. [30] proposed a Burton-Miller-type SBM (BM-SBM), which allows the method to accurately and stably solve acoustic radiation and scattering problems. Compared with other traditional methods, the BM-SBM is free of integration and mesh, mathematically simple and easy to program. Meanwhile, the combination of the Burton-Miller formula and the SBM overcomes the non-uniqueness issue in the vicinity of the corresponding interior eigenfrequencies, and it has been effectively verified on the acoustic radiation and scattering problems.

The coefficient matrices of the BEM, MFS and BM-SBM each constitute asymmetric dense full-rank matrices with storage memory represented by $O(N^2)$, where N is the number of computational domain nodes. If a large-scale problem with millions of degrees of freedom is considered, it is indeed difficult for a computer to solve. As a result, many scholars have conducted research on fast algorithms in order to efficiently solve large-scale problems [31–33]. Currently, fast algorithms can be classified into three main categories based on mathematical principles: the fast Fourier transform [34,35] algorithm, the fast multipole method [36] and algebraic methods based on matrix compression.

Among the algebraic methods based on matrix compression, Hackbusch and Khoromskij [37,38]

proposed the theory of the hierarchical matrix (H-matrix) in one-dimensional space. The idea of the H-matrix is to sparsely represent the coefficient matrix. The H-matrix has nearly linear complexity in matrix operations such as matrix-vector multiplication, matrix-matrix multiplication and matrix inversion. It divides the entire coefficient matrix into two types of matrix blocks according to the allowable conditions: one is the block of far-field sub-matrices that can be represented approximately and the other is the block of near-field sub-matrices that needs to be stored and expressed completely. In addition, Bebendorf and Rjasanow [39,40] developed the theoretical formulation of the adaptive cross-approximation (ACA) algorithm based on the pseudo-skeleton approximation, ultimately proving the higher robustness of the ACA method in the low-rank approximation process.

In this paper, ACA is introduced into the BM-SBM to accelerate the solving process for the acoustic sensitivity associated with external sound fields subject to Dirichlet and Neumann boundary conditions. Unlike the conventional BM-SBM, the proposed ACA-BM-SBM uses low-rank approximation instead of the traditional iterative solution and Gaussian elimination, which greatly improves computational efficiency and reduces the memory requirement. Therefore, the proposed method has great potential in the acoustic sensitivity analysis of large-scale problems.

The rest of this paper is organized as follows. Section 2 briefly describes the acoustic sensitivity problem, and, in Section 3, the conventional SBM and the BM-SBM are described. In Section 4, the principle of the ACA algorithm and the calculation steps are given. In Section 5, four examples are provided to illustrate the efficiency and accuracy of the proposed algorithm. Finally, some conclusions are summarized in Section 6.

2. Acoustic sensitivity analysis

Consider a general twodimensional sound propagation problem governed by

$$\nabla^2 u(\boldsymbol{x}) + k^2 u(\boldsymbol{x}) = 0, \quad \boldsymbol{x} = (x_1, x_2) \in \Omega, \tag{1}$$

subject to the following Dirichlet and Neumann boundary conditions:

$$u(\boldsymbol{x}) = \bar{u}(\boldsymbol{x}), \quad \boldsymbol{x} = (x_1, x_2) \in \Gamma_{\mathrm{D}}, \tag{2}$$

$$q(\boldsymbol{x}) = \frac{\partial u(\boldsymbol{x})}{\partial \boldsymbol{n}_x}, \quad \boldsymbol{x} = (x_1, x_2) \in \Gamma_{\mathrm{N}}, \tag{3}$$

where ∇^2 represents the Laplace operator, $u(\boldsymbol{x})$ denotes the sound pressure value of point $\boldsymbol{x}$ in the external sound field, $k = 2\pi f / c$ indicates the wave number, f refers to the sound frequency, c is the medium velocity in the external field, and $\bar{u}(\boldsymbol{x})$ and $\dfrac{\partial u(\boldsymbol{x})}{\partial \boldsymbol{n}_x}$ are the known sound pressure and its normal derivative on boundaries Γ_{D} and Γ_{N}, respectively. The acoustic sensitivity in this paper can be expressed as

$$\dot{u}(\boldsymbol{x}) = \dot{\bar{u}}(\boldsymbol{x}), \quad \boldsymbol{x} \in \Gamma_{\mathrm{D}}, \tag{4}$$

$$\dot{q}(\boldsymbol{x}) = \dot{\bar{q}}(\boldsymbol{x}), \quad \boldsymbol{x} \in \Gamma_{\mathrm{N}}, \tag{5}$$

where $\dot{u}(\boldsymbol{x})$ and $\dot{q}(\boldsymbol{x})$ denote the differentiation of physical quantities with respect to the design variables, and $\dot{\bar{u}}(\boldsymbol{x})$ and $\dot{\bar{q}}(\boldsymbol{x})$ indicate known values.

For two-dimensional external acoustic field problems, the sound pressure should satisfy the condition at infinity, i.e., the Sommerfeld condition [41]:

$$\lim_{r\to\infty} r^{\frac{1}{2}}\left[\frac{\partial u(\boldsymbol{x})}{\partial r} - \mathrm{i}ku(\boldsymbol{x})\right] = 0, \tag{6}$$

where r denotes the distance from the point $\boldsymbol{x}$ to the center of the acoustic field, and i is an imaginary unit.

3. Burton-Miller-type singular boundary method

The SBM is a semi-analysis boundary-type meshless method. It represents the sound pressure at the true boundary point as a linear accumulation of the fundamental solution, while introducing the concept of OIFs to avoid the source singularity problem caused by the coincidence of field and source points, as shown in Figure 1.

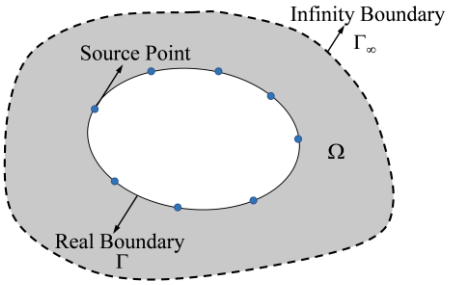

Figure 1. Distribution of source points for external acoustic problems.

The solutions $u(\boldsymbol{x})$ and $q(\boldsymbol{x})$ of the SBM are approximated as a linear accumulation based on the fundamental solutions of all collocation points, namely,

$$u(\boldsymbol{x}_i) = \sum_{j=1, i\neq j}^{N} \alpha_j G(\boldsymbol{x}_i, \boldsymbol{s}_j) + \alpha_i u_{ii}, \quad \boldsymbol{x}_i \in \Gamma_{\mathrm{D}}, \boldsymbol{s}_j \in \Gamma, \tag{7}$$

$$q(\boldsymbol{x}_i) = \sum_{j=1, i\neq j}^{N} \alpha_j \frac{\partial G(\boldsymbol{x}_i, \boldsymbol{s}_j)}{\partial \boldsymbol{n}_x} + \alpha_i q_{ii}, \quad \boldsymbol{x}_i \in \Gamma_{\mathrm{N}}, \boldsymbol{s}_j \in \Gamma, \tag{8}$$

where α_j represents the unknown coefficient corresponding to the jth source point, $\boldsymbol{x}_i$ denotes the ith field point and $\boldsymbol{s}_j$ denotes the jth source point; N is the number of source points or field points, both of which are equal. In addition, u_{ii} and q_{ii} are the OIFs for the Dirichlet and Neumann

boundary conditions, respectively. $G(\boldsymbol{x}_i,\boldsymbol{s}_j)$ refers to the fundamental solution to the Helmholtz equation:

$$G(\boldsymbol{x}_i,\boldsymbol{s}_j)=\frac{\mathrm{i}}{4}H_0^{(1)}\left(kr(\boldsymbol{x}_i,\boldsymbol{s}_j)\right), \tag{9}$$

where $r(\boldsymbol{x}_i,\boldsymbol{s}_j)$ denotes the distance between the filed point $\boldsymbol{x}_i$ and the source point $\boldsymbol{s}_j$; $H_0^{(1)}$ represents the Hankel function of the first kind of order zero, and its derivative is as follows:

$$\frac{\mathrm{d}H_0^{(1)}(w)}{\mathrm{d}w}=\frac{\mathrm{d}J_0(w)}{\mathrm{d}w}+\mathrm{i}\frac{\mathrm{d}Y_0(w)}{\mathrm{d}w}=-J_1(w)+\frac{\mathrm{i}}{2}\left(Y_{-1}(w)-Y_1(w)\right), \tag{10}$$

where J_0 and Y_0 represents the zero-order Bessel function of the first kind and the second kind, respectively.

In order to address the fictitious frequency issues in acoustic sensitivity analysis, the BM-SBM formulations based on Eqs (7) and (8) are given as follows:

$$u(\boldsymbol{x}_i)=\sum_{j=1,i\neq j}^{N}\alpha_j\left(G(\boldsymbol{x}_i,\boldsymbol{s}_j)+\eta\frac{\partial G(\boldsymbol{x}_i,\boldsymbol{s}_j)}{\partial \boldsymbol{n}_s}\right)+\alpha_i u_{ii}^{\mathrm{BM}},\ \boldsymbol{x}_i\in\Gamma_{\mathrm{D}},\boldsymbol{s}_j\in\Gamma, \tag{11}$$

$$q(\boldsymbol{x}_i)=\sum_{j=1,i\neq j}^{N}\alpha_j\left(\frac{\partial G(\boldsymbol{x}_i,\boldsymbol{s}_j)}{\partial \boldsymbol{n}_x}+\eta\frac{\partial^2 G(\boldsymbol{x}_i,\boldsymbol{s}_j)}{\partial \boldsymbol{n}_s\partial \boldsymbol{n}_x}\right)+\alpha_i q_{ii}^{\mathrm{BM}},\ \boldsymbol{x}_i\in\Gamma_{\mathrm{N}},\boldsymbol{s}_j\in\Gamma, \tag{12}$$

where $\eta=1/(k+1)$, and u_{ii}^{BM} and q_{ii}^{BM} are OIFs of the BM-SBM.

The OIFs in Eqs (7) and (8) constitute the core part of the SBM. By using the empirical formulas, u_{ii} and q_{ii} are written as follows [42,43]:

$$u_{ii}=\frac{\mathrm{i}}{4}-\frac{1}{2\pi}\left(\ln(\frac{l_j}{2\pi})+\ln(\frac{k}{2})+\varepsilon\right), \tag{13}$$

$$q_{ii}=\frac{1}{l_j}-\sum_{j=1,j\neq i}^{N}\frac{l_j}{l_i}\frac{\partial G_{\mathrm{L}}(\boldsymbol{x}_i,\boldsymbol{s}_j)}{\partial \boldsymbol{n}_s}, \tag{14}$$

where l_j is the influence range of the source points, as shown in Figure 2, ε is the Euler constant and $G_{\mathrm{L}}(\boldsymbol{x}_i,\boldsymbol{s}_j)=-\ln\left|\boldsymbol{x}_i-\boldsymbol{s}_j\right|/(2\pi)$ represents the fundamental solution of the Laplace equation.

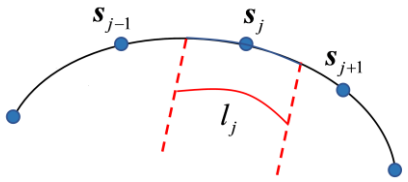

Figure 2. Influence range of source points for two-dimensional problems.

For the problem of acoustic sensitivity in the infinite domain, the OIFs corresponding to the BM-SBM are as follows:

$$u_{ii}^{\mathrm{BM}} = u_{ii} - \eta \sum_{j=1, j\neq i}^{N} \frac{l_j}{l_i} \frac{\partial G_{\mathrm{L}}(\boldsymbol{x}_i, \boldsymbol{s}_j)}{\partial \boldsymbol{n}_s}, \tag{15}$$

$$q_{ii}^{\mathrm{BM}} = q_{ii} + \eta \left(\frac{k^2}{2} u_{ii} - \sum_{j=1, j\neq i}^{N} \frac{l_j}{l_i} \frac{\partial^2 G_{\mathrm{L}}(\boldsymbol{x}_i, \boldsymbol{s}_j)}{\partial \boldsymbol{n}_s \partial \boldsymbol{n}_x} \right). \tag{16}$$

Substituting the boundary conditions into Eqs (11) and (12), the following system of linear equations can be written:

$$\mathbf{A}\boldsymbol{\alpha} = \mathbf{b}, \tag{17}$$

where $\mathbf{A}$ is the coefficient matrix of the BM-SBM, $\boldsymbol{\alpha}$ denotes the coefficient vector to be solved and $\mathbf{b}$ is the known boundary condition of the problem. It should be pointed out that the traditional methods need to generate the matrix $\mathbf{A}$ and solve Eq (17) by employing iterative or direct solvers. However, we will develop a new matrix compression technique in Section 4 to obtain the coefficient vector $\boldsymbol{\alpha}$ based on the ACA algorithm.

After obtaining $\boldsymbol{\alpha}$, the sound pressure and the acoustic sensitivity at any point in the acoustic field can be respectively expressed as

$$u(\boldsymbol{x}) = \sum_{j=1}^{N} \alpha_j \left(G(\boldsymbol{x}, \boldsymbol{s}_j) + \eta \frac{\partial G(\boldsymbol{x}, \boldsymbol{s}_j)}{\partial \boldsymbol{n}_s} \right), \quad \boldsymbol{x} \in \Omega, \boldsymbol{s}_j \in \Gamma, \tag{18}$$

$$\dot{u}(\boldsymbol{x}) = \sum_{j=1}^{N} \begin{bmatrix} \dot{\alpha}_j \left(G(\boldsymbol{x}, \boldsymbol{s}_j) + \eta \dfrac{\partial G(\boldsymbol{x}, \boldsymbol{s}_j)}{\partial \boldsymbol{n}_s} \right) + \\ \alpha_j \left(\dot{G}(\boldsymbol{x}, \boldsymbol{s}_j) + \dot{\eta} \dfrac{\partial G(\boldsymbol{x}, \boldsymbol{s}_j)}{\partial \boldsymbol{n}_s} + \eta \dfrac{\partial \dot{G}(\boldsymbol{x}, \boldsymbol{s}_j)}{\partial \boldsymbol{n}_s} \right) \end{bmatrix}, \quad \boldsymbol{x} \in \Omega, \boldsymbol{s}_j \in \Gamma, \tag{19}$$

where $\dot{\alpha}_j$ and $\dot{G}(\boldsymbol{x}, \boldsymbol{s}_j)$ denote the differentiation of α_j and $G(\boldsymbol{x}, \boldsymbol{s}_j)$, respectively, for the design variables. $\dot{\lambda} = -\mathrm{i}/(k+1)^2$ when the design variable is the wave number k. The vector form of Eq (19) can be written as follows:

$$\dot{\mathbf{u}} = \dot{\boldsymbol{\alpha}} \left(\mathbf{G} + \eta \frac{\partial \mathbf{G}}{\partial \mathbf{n}} \right) + \boldsymbol{\alpha} \left(\dot{\mathbf{G}} + \dot{\eta} \frac{\partial \mathbf{G}}{\partial \mathbf{n}} + \eta \frac{\partial \dot{\mathbf{G}}}{\partial \mathbf{n}} \right). \tag{20}$$

Taking the wave number k as an example, since α_j cannot be differentiated directly with respect to k, the three-point difference method is used to approximate $\dot{\alpha}_j$, as shown in the following equation:

$$\begin{cases} \dot{\alpha}_j(t_k) \approx \dfrac{1}{2\Delta t}\left(-3\alpha_j(t_k) + 4\alpha_j(t_{k+1}) - \alpha_j(t_{k+2})\right), \\ \dot{\alpha}_j(t_{k+1}) \approx \dfrac{1}{2\Delta t}\left(\alpha_j(t_{k+2}) - \alpha_j(t_k)\right), \\ \dot{\alpha}_j(t_{k+2}) \approx \dfrac{1}{2\Delta t}\left(\alpha_j(t_k) - 4\alpha_j(t_{k+1}) + 3\alpha_j(t_{k+2})\right). \end{cases} \tag{21}$$

4. Adaptive cross-approximation

The system of the linear Eq (17) in Section 3 has the computational complexity of $O(N^2)$. More storage memory and computation time are required when solving large-scale systems; hence, the ACA algorithm is introduced in this section [44,45].

The core of the ACA algorithm is the low-rank compression of sub- matrices of the large matrix **A**. Before that, how to decompose the large matrix **A** into sub-matrices should be considered. When decomposing the matrix **A**, the clustered and partitioned points are stored in the index subsets of the quadtree based on the geometric location of the source points.

The admissible condition is an important basis for distinguishing between near blocks and far blocks, where near blocks need to be fully expressed while far blocks are compressed by using the ACA algorithm to achieve matrix sparsity. The traditional admissible condition is written as

$$\min\{\mathrm{diam}(\Omega_t), \mathrm{diam}(\Omega_s)\} \le \eta \mathrm{dist}(\Omega_t, \Omega_s), \tag{22}$$

where Ω_t and Ω_s are two source point clusters, $\mathrm{diam}(\cdot)$ denotes the diameter range of the space, $\mathrm{dist}(\cdot)$ denotes the distance between two spaces and $0 < \eta < 1$ is the compatibility condition factor. The mathematical form of the traditional admissible condition is simple, but the calculations of $\mathrm{diam}(\cdot)$ and $\mathrm{dist}(\cdot)$ require a computational size of $O(N^2)$. To avoid the above problem, Wei et al. [46] introduced the background grid to cluster points and generate the list of admissible cluster pairs (Figure 3). Depending on the number of levels in the tree structure, each cell comprising the grids has a corresponding index (*i*, *j*), and the distribution points are located in all cells. Taking Figure 3 for example, the cell {1, 2, 3, 4} in level 2, the cell {1,2} in level 3 and the cell {1} in level 4 are indexed as (1,1), (2,1) and (4,1), respectively. The new admissible condition, rather than Eq (21), is written as

$$\left|i_{\Omega_t} - i_{\Omega_s}\right| > \mu \text{ and } \left|j_{\Omega_t} - j_{\Omega_s}\right| > \mu, \tag{23}$$

where μ is a pre-set positive integer.

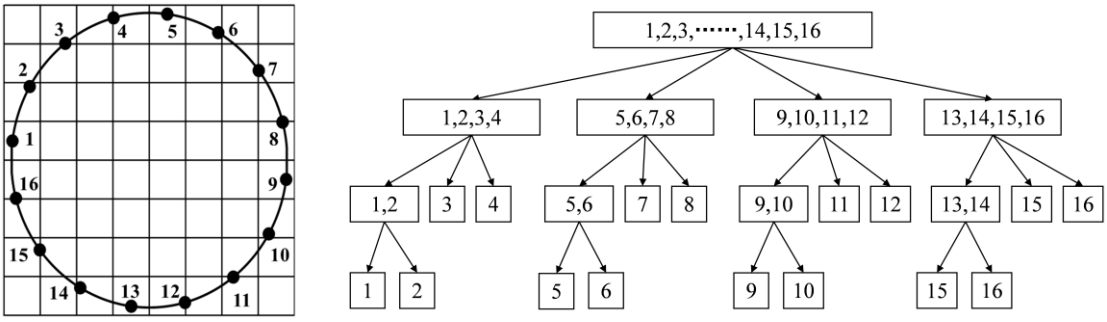

Figure 3. Diagrams of the cluster (left) and quadtree (right).

The hierarchical matrix is shown in Figure 4 for $\mu = 1$. As shown in Figure 4, the new admissible condition only requires the index number; thus, no extra calculations are needed to generate the admissible cluster pairs. Then, the far-field block $\mathbf{B}^{m\times n}$ which meets the admissible condition can be approximated by using low-rank methodology, as follows: $\mathbf{U}^{m\times r}\mathbf{V}^{r\times n}$ (Figure 5). The major steps for the ACA algorithm are shown in Figure 6.

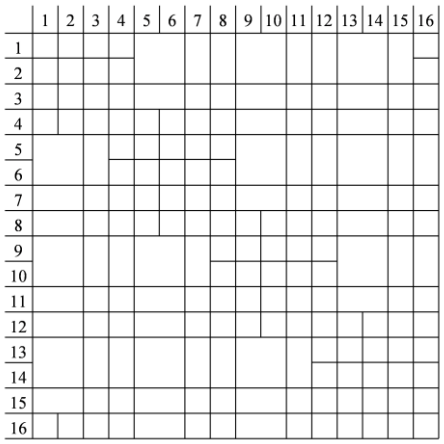

Figure 4. The hierarchical matrix ($\mu = 1$).

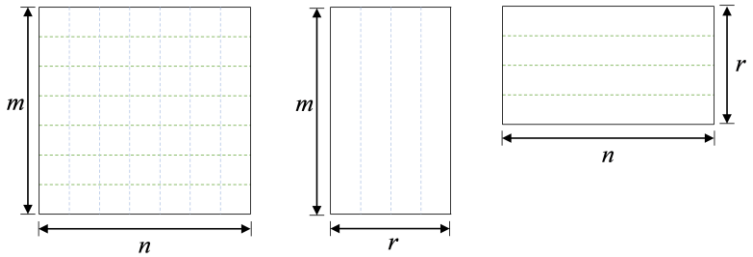

Figure 5. The diagram of the ACA matrix approximate decomposition.

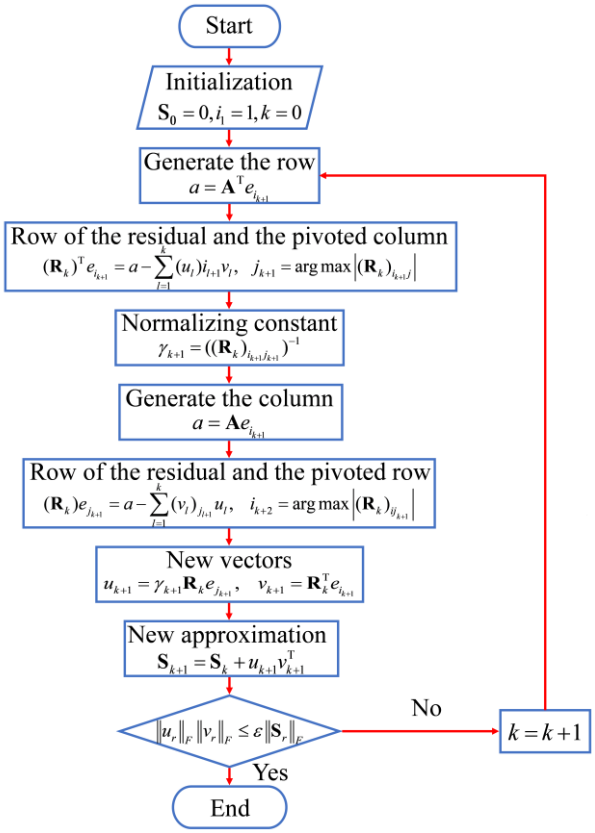

Figure 6. The steps for the ACA algorithm.

5. Numerical results and discussions

In this section, four examples are presented to verify the accuracy and effectiveness of the proposed method. Numerical accuracy is judged by the relative root mean square error (RRMSE):

$$\mathrm{RRMSE}=\frac{\sqrt{\sum_{j=1}^{M}\left(\dot{u}_{\mathrm{n}}(t_j)-\dot{u}_{\mathrm{e}}(t_j)\right)^2}}{\sqrt{\sum_{j=1}^{M}\dot{u}_{\mathrm{e}}(t_j)^2}}, \tag{24}$$

where t_j denotes the jth value of M equidistant nodes for the design variable; $\dot{u}_{\mathrm{n}}(t_j)$ and $\dot{u}_{\mathrm{e}}(t_j)$ respectively indicate the numerical and exact solutions at the design variable t_j. The computing platform in this study was a Windows 10 (64 bit) laptop with a 2.3 GHz CPU and 16 GB RAM, coded in MATLAB.

5.1. Acoustic radiation by an infinite pulsating cylinder (Neumann boundary condition)

An infinite pulsating cylinder is considered [43]. The analytical solution of the sound pressure at the external acoustic field for an infinite pulsating cylinder is as follows:

$$u(r)=\frac{\mathrm{i}\rho c v_0 H_0^1(kr)}{H_1^1(ka)}, \tag{25}$$

where $v_0=1\mathrm{m/s}$ is the velocity of the normal vibration, r is the distance from the test point to coordinates (0,0), and $\rho=1.2\ \mathrm{kg/m^3}$ and $c=341\ \mathrm{m/s}$ are the density of air and the speed of propagation of sound waves in air, respectively. The exact solution for the acoustic sensitivity with respect to the wave number k can be expressed as

$$\frac{\partial u}{\partial k}=\frac{-\mathrm{i}\rho c v_0}{\left(H_1^1(ka)\right)^2}\left[rH_1^1(kr)H_1^1(ka)+\frac{a}{2}H_0^1(kr)\left(H_0^1(ka)-H_2^1(ka)\right)\right]. \tag{26}$$

A pulsating cylinder with radius $a=1\mathrm{m}$ is investigated and $N=100000$ uniformly distributed source points were chosen on the boundary. The frequency f was divided into 100 design variables from 50 Hz to 300 Hz, i.e., the wave number $k=2\pi f/c$ rises from 0.92 to 5.53 at intervals of $\Delta k=0.0465$.

Figure 7 shows that the numerical results of sensitivity obtained by the FEM, the BM-SBM and the ACA-BM-SBM agree in agreement very well with the exact solutions when $N=6000$. The RRMSEs of acoustic sensitivity for the real part corresponding to the FEM, the BM-SBM and the ACA-BM-SBM were 0.0066, 0.0010 and 0.0011, respectively. Similarly, the results of the above method in the imaginary part were 0.0068, 0.0012 and 0.0013, respectively. The last two methods were superior to the FEM in terms of computational accuracy, and the BM-SBM was slightly better than the ACA-BM-SBM. The relative errors between the ACA-BM-SBM and the exact solution are also provided in Figure 8 for $N=100000$, which verifies the accuracy of this acceleration algorithm. In addition, Figure 9 shows the histograms of the CPU computation time of the traditional BM-SBM and the proposed ACA-BM-SBM, indicating that the ACA algorithm can save plenty of time in the computation of large-scale matrices. In addition, Figure 10 displays the RRMSEs of these two methods, as obtained for different numbers of source points. It can be seen that the two methods have good convergence, while the traditional BM-SBM faces the issue of limited computer memory when solving large-scale problems.

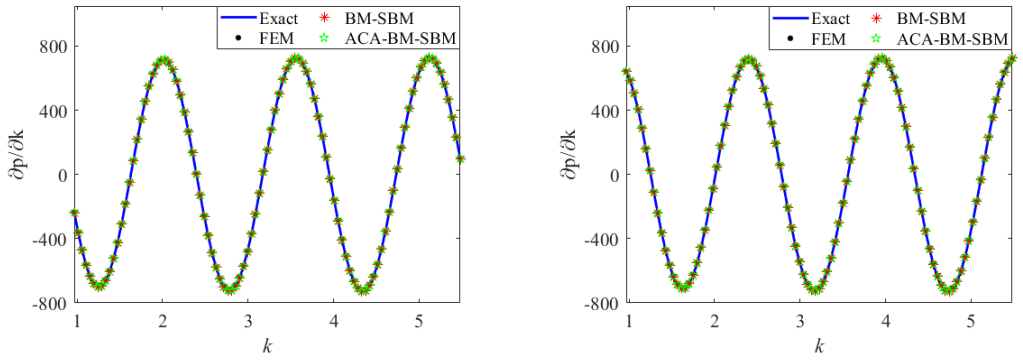

(a) Real part (b) Imaginary part

Figure 7. Comparisons of numerical and exact solutions for the pulsating cylinder (N = 6000).

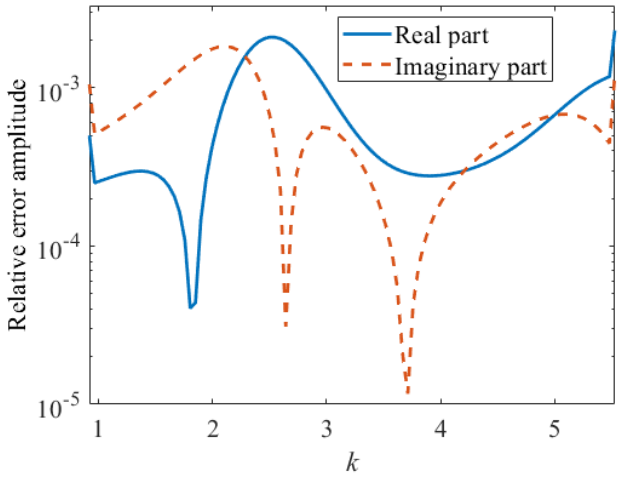

Figure 8. Relative errors of real and imaginary parts ($N = 100000$).

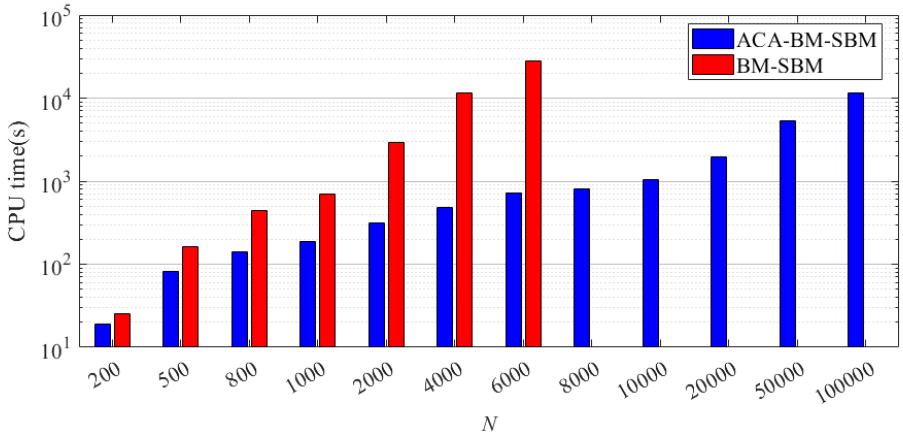

Figure 9. The CPU times of the ACA-BM-SBM and BM-SBM.

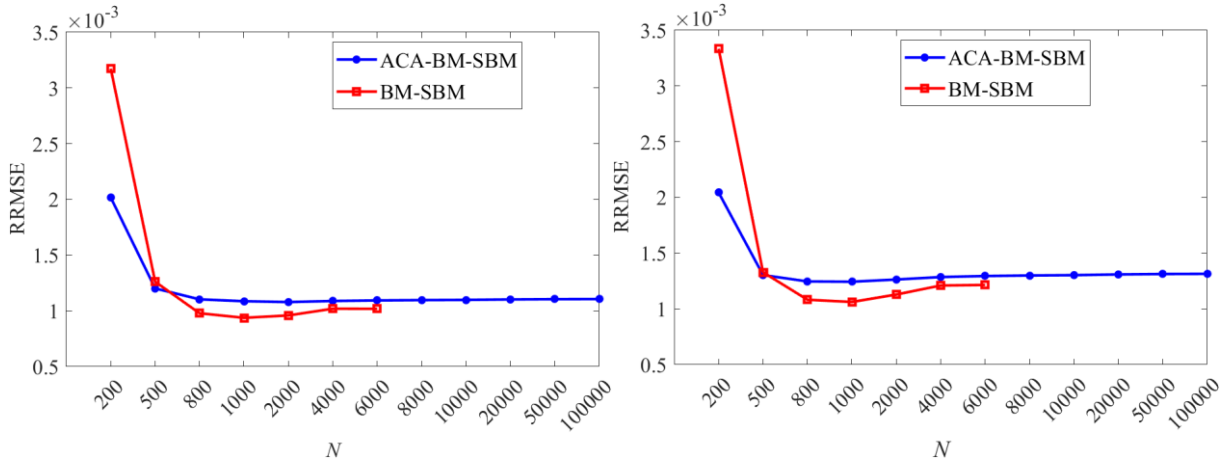

(a) Real part (b) Imaginary part

Figure 10. The RRMSEs of the ACA-BM-SBM and BM-SBM for different numbers of source points.

5.2. Acoustic scattering by a rigid cylinder (Neumann boundary condition)

In the second example, the scattering of a rigid cylinder in a planar acoustic background is considered, as shown in Figure 11. The wave number k is the design variable for acoustic sensitivity analysis. The exact solution for sensitivity is

$$\frac{\partial u}{\partial k} = -k\sum_{n=0}^{\infty} \mathrm{i}^n \left(J_{(n-1)}(ka) - J_{(n+1)}(ka) \right) \cos(n\theta). \tag{27}$$

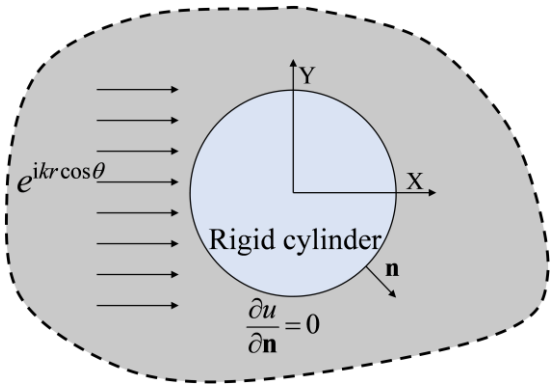

Figure 11. The rigid cylinder scattering model.

Figure 12 illustrates the comparisons of the numerical and exact solutions of acoustic sensitivity with respect to wave number for the rigid cylinder when the number of source points is set as N = 10000. From this figure, we can find that the ACA-BM-SBM can accurately and effectively predict the acoustic sensitivity of the considered rigid cylinder.

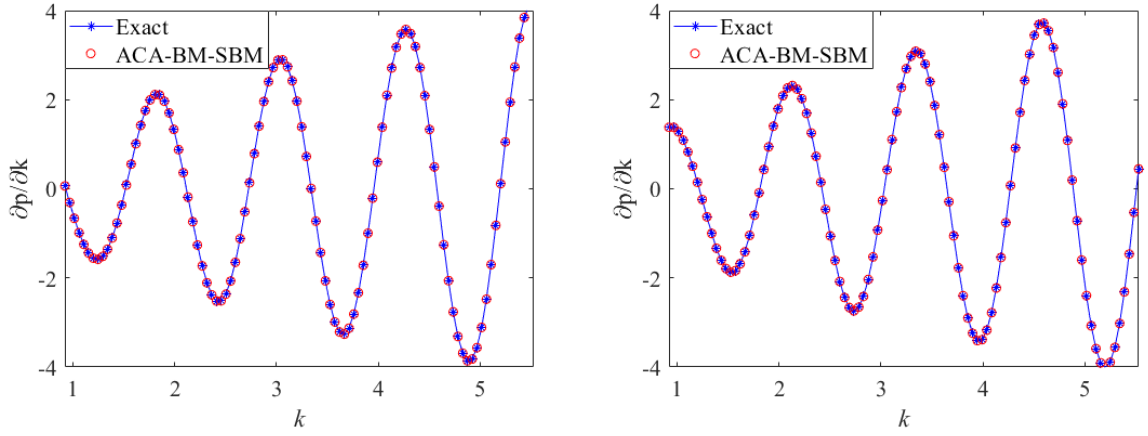

(a) Real part (b) Imaginary part

Figure 12. Comparisons of numerical and exact solutions for the rigid cylinder (N = 10000).

Table 1 lists the condition numbers and memories of the conventional BM-SBM and the ACA-BM-SBM for various numbers of boundary nodes. The condition number increased with the increasing

number of nodes, and it still had a relatively smaller value. As the number of boundary nodes increases, the memory required by the conventional BM-SBM increases dramatically, eventually leading to insufficient memory for computation. In contrast, the ACA-BM-SBM requires less memory under the same conditions; thus, calculations for large-scale problems can be performed.

Table 1. Condition numbers and memories of the conventional BM-SBM and the ACA-BM-SBM for various numbers of boundary nodes.

Boundary nodes N	Condition number	Memory (MB)	
		Conventional BM-SBM	ACA-BM-SBM
200	7.41	0.61	0.45
500	18.26	3.81	1.96
800	29.12	9.77	3.20
1000	36.37	15.26	4.46
2000	72.59	61.04	10.22
4000	145.06	244.14	23.70
6000	217.52	549.32	39.52
8000	——	——	53.95
10000	——	——	70.88
20000	——	——	155.00
50000	——	——	437.96
100000	——	——	927.57

5.3. Acoustic scattering by a rigid cylinder (Neumann boundary condition)

This example considers a sound scattering problem from a car-like model, as shown in Figure 13. Obviously, this is a half-space problem. We assume that there is a sound source at the rear of the car, and this sound source can be represented as

$$P_{\text{in}} = \frac{\text{i}}{4} H_0^{(1)}\left(k \cdot r_{\text{obs}}\right) + \frac{\text{i}}{4} H_0^{(1)}\left(k \cdot r_{\text{sym}}\right), \tag{28}$$

where r_{obs} denotes the distance between all boundary points of the car-like model and the sound source, r_{sym} represents the distance between all boundary points of the car-like model that are symmetrical about the X axis and the sound source. The calculation formula for the sound pressure level is given as

$$SPL = 20\log_{10}\left(\frac{|p|}{p_0}\right), \tag{29}$$

where p is the sound pressure at the test point and p_0 is the reference sound pressure, usually taken as $2.0\times10^{-5}\,\text{Pa}$.

The acoustic sensitivity with respect to the wave number k can be calculated as follows:

$$\frac{\partial \mathbf{u}}{\partial k}=\frac{\partial \boldsymbol{\alpha}}{\partial k}\left(\mathbf{G}+\eta\frac{\partial \mathbf{G}}{\partial \mathbf{n}}\right)+\boldsymbol{\alpha}\left(\frac{\partial \mathbf{G}}{\partial k}+\frac{\partial \eta}{\partial k}\frac{\partial \mathbf{G}}{\partial \mathbf{n}}+\eta\frac{\partial^2 \mathbf{G}}{\partial \mathbf{n}\partial k}\right)+\frac{\partial P_{\text{in}}}{\partial k}. \tag{30}$$

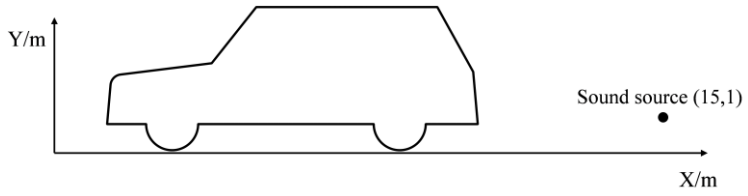

Figure 13. The car-like model in a half-space.

Since there is no exact solution for this problem, the simulation results for the FEM obtained via COMSOL Multiphysics were used as reference values. Figure 14 compares the distributions of sound pressure levels with various frequencies obtained from the ACA-BM-SBM and the FEM. It is observed that the numerical solutions of the two methods are very consistent, and the deviations at 100 Hz, 200 Hz and 300 Hz are respectively 0.36, 0.32 and 0.31 by calculation, proving the effectiveness of the ACA-BM-SBM. Finally, Figure 15 gives the numerical results of acoustic sensitivity for the three test points A (8, 8), B (8, 5) and C (2, 5). The acoustic sensitivity deviations between the FEM and the ACA-BM-SBM in the real part are 0.0502, 0.0128 and 0.0157, respectively, for the above three test points. And, the deviation results for the imaginary part are 0.0525, 0.0122 and 0.0173, respectively.

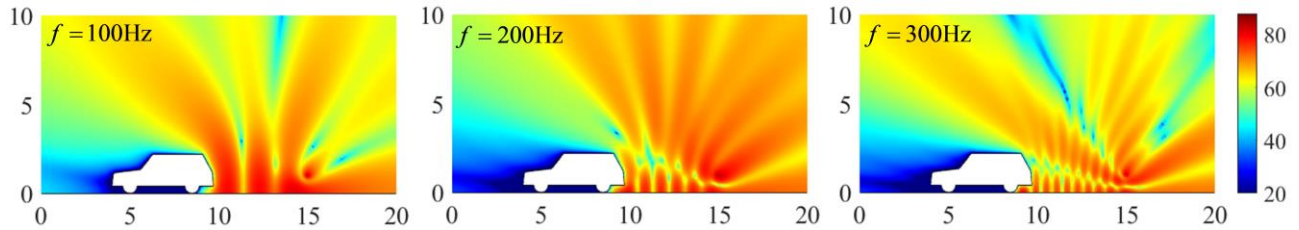

(a) ACA-BM-SBM

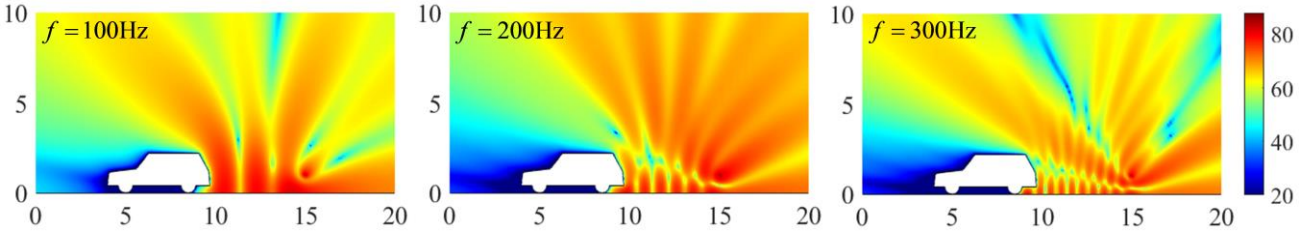

(b) FEM

Figure 14. Comparisons of sound pressure levels obtained by the ACA-BM-SBM and the FEM.

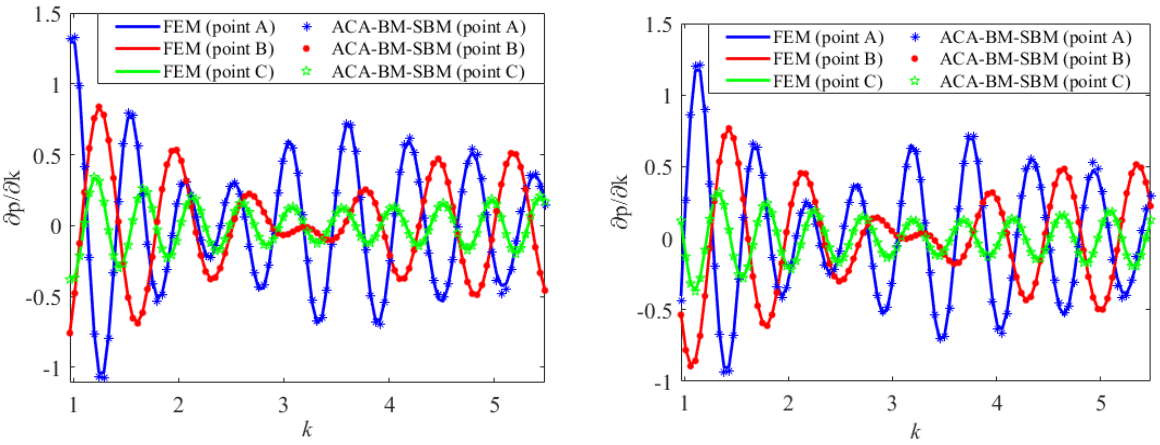

(a) Real part (b) Imaginary part

Figure 15. Acoustic sensitivities of the real and imaginary parts at points A, B and C.

5.4. Acoustic scattering by a square plate with multiple holes (Dirichlet boundary condition)

The last example considers a square plate containing 100 circular holes, as shown in Figure 16. In the calculation, the ACA-BM-SBM used N = 20000 boundary nodes, from which an evenly distributed set of 200 nodes on each circle were chosen.

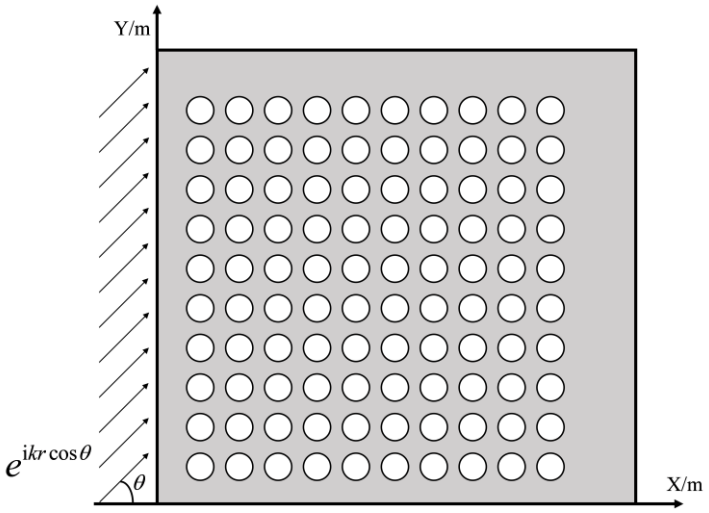

Figure 16. The square plate with 100 multi-connected domains in a plane wave.

Figure 17 shows the profiles of the sound pressure on the square [0, 4]×[0, 4] obtained by employing the proposed fast algorithm and the FEM with different plane wave incidence angles and different frequencies. It can be noticed from Figure 17 that the numerical results of the ACA-BM-SBM agree well with those of the FEM obtained via COMSOL Multiphysics. Numerical experiments indicate that the proposed scheme can address the large-scale and multi-connected problem accurately and effectively.

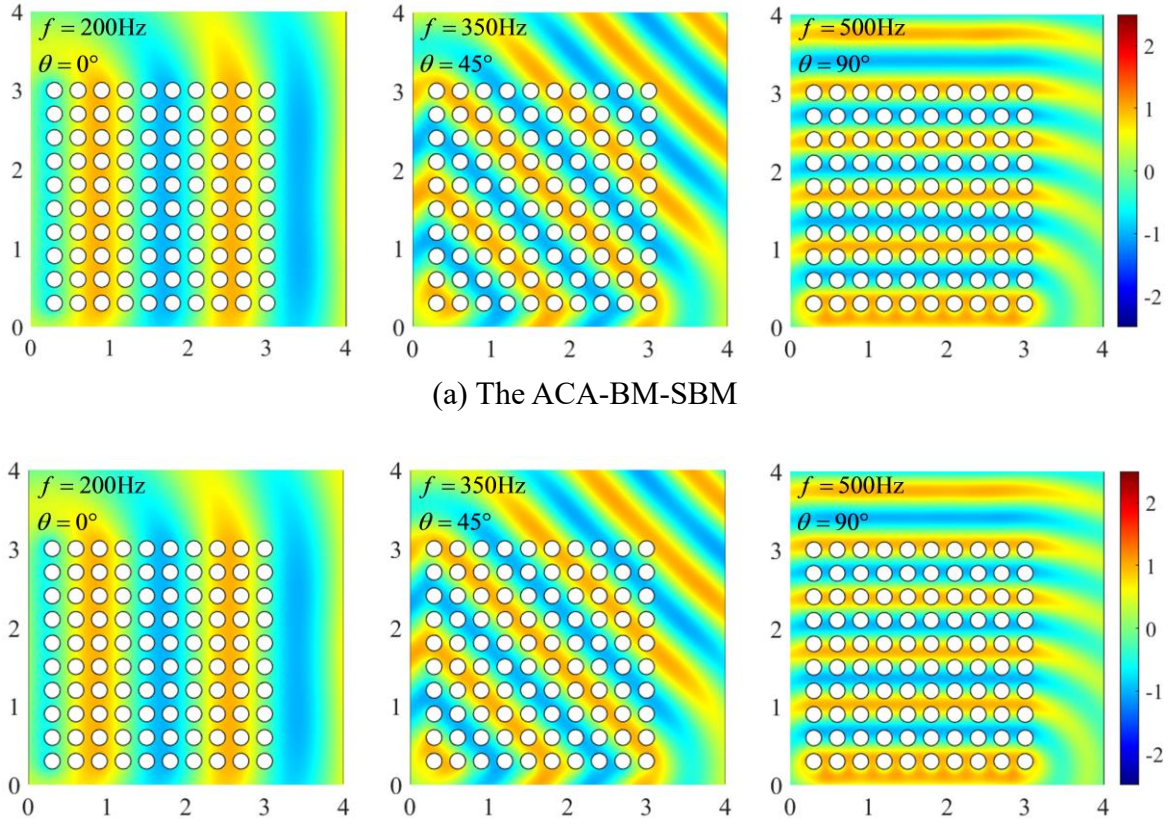

(a) The ACA-BM-SBM

(b) The FEM

Figure 17. Sound pressure values for three incident wave angles and frequencies.

To analyze the sensitivity of this problem and provide data for the validation of other numerical methods, Figure 18 was constructed to provide the predicted values of the acoustic sensitivity with respect to the wave number at the three test points D (3, 3.5), E (3.5, 1) and F (2, 3.5). The acoustic sensitivity deviations between the FEM and the ACA-BM-SBM in the real part are 0.00497, 0.00223 and 0.00345, respectively, for the above three test points. The deviation results for the imaginary part are 0.00496, 0.00224 and 0.00350, respectively.

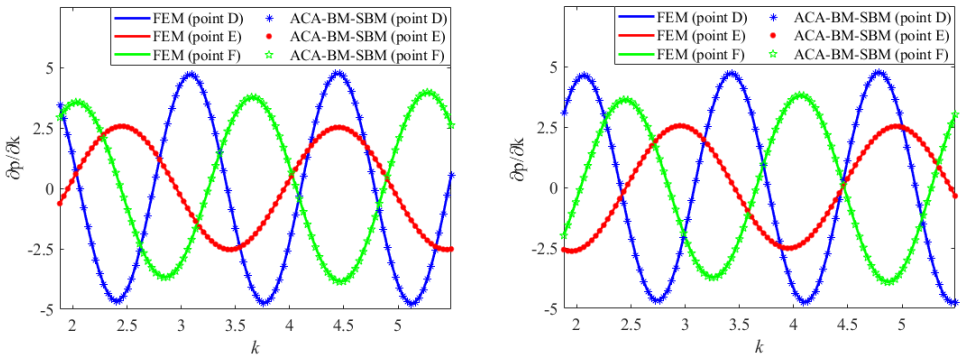

(a) Real part

(b) Imaginary part

Figure 18. Numerical results for acoustic sensitivity at the points D, E and F.

6. Conclusions

We have proposed a fast meshless approach called the ACA-BM-SBM for acoustic sensitivity analysis by introducing ACA into the BM-SBM. Compared with the BEM and the MFS, the new method avoids singular integrals and a fictitious boundary, and thus is simple and straightforward. More importantly, the developed ACA-BM-SBM circumvents the solution of dense matrices by adopting the matrix compression technique, resulting in a fast calculation process. Based on this, the new method has the potential to become a tool for the large-scale simulation of acoustic sensitivity analysis.

Numerical examples have been provided to investigate the acoustic radiation from an infinite pulsating cylinder, acoustic scattering by a rigid cylinder, acoustic scattering by a car-like model in a half-plane and plane wave scattering in a multi-connected domain. Results demonstrate that the proposed method is accurate, efficient and convergent for acoustic sensitivity analysis with various geometries and boundary conditions. This study provides a numerical tool for acoustic sensitivity analysis with complicated structures; it also lays the foundation for the acoustic structure optimization in the future.

It should be pointed out that the ACA-BM-SBM proposed in this paper is only applicable to 2D problems. In theory, this method can be directly extended to 3D cases, which will be an important part of our future research. In addition, we chose to employ the direct differentiation method in the acoustic sensitivity analysis, which is time-consuming and labor-intensive for multiple design variables. Therefore, our future work will focus on the topological optimization of acoustic structures under the premise of solving 3D problems and achieving acceleration.

Use of AI tools declaration

The authors declare that they have not used artificial intelligence tools in the creation of this article.

Acknowledgments

The work described in this paper was supported by the Natural Science Foundation of Shandong Province of China (Grant No. ZR2023YQ005).

Conflict of interest

The authors declare no conflict of interest.

References

1. H. Liu, F. Wang, A novel semi-analytical meshless method for the thickness optimization of porous material distributed on sound barriers, *Appl. Math. Lett.*, **147** (2024), 108844. https://doi.org/10.1016/j.aml.2023.108844
2. L. Chen, C. Liu, W. Zhao, L. Liu, An isogeometric approach of two dimensional acoustic design sensitivity analysis and topology optimization analysis for absorbing material distribution, *Comput. Meth. Appl. Mech. Eng.*, **336** (2018), 507–532. https://doi.org/10.1016/j.cma.2018.03.025

3. D. Fritze, S. Marburg, H. J. Hardtke, FEM-BEM-coupling and structural-acoustic sensitivity analysis for shell geometries, *Comput. Struct.*, **83** (2005), 143–154. https://doi.org/10.1016/j.compstruc.2004.05.019
4. N. H. Kim, J. Dong, K. K. Choi, N. Vlahopoulos, Z. D. Ma, M. Castanier, et al., Design sensitivity analysis for sequential structural-acoustic problems, *J. Sound Vibr.*, **263** (2003), 569–591. https://doi.org/10.1016/S0022-460X(02)01067-2
5. L. Magri, M. P. Juniper, Sensitivity analysis of a time-delayed thermo-acoustic system via an adjoint-based approach, *J. Fluid Mech.*, **719** (2013), 183–202. https://doi.org/10.1017/jfm.2012.639
6. L. Chen, C. Zheng, H. Chen, FEM/wideband FMBEM coupling for structural-acoustic design sensitivity analysis, *Comput. Meth. Appl. Mech. Eng.*, **276** (2014), 1–19. https://doi.org/10.1016/j.cma.2014.03.016
7. T. Wang, R. Green, R. Guldiken, J. Wang, S. Mohapatra, S. S. Mohapatra, Finite element analysis for surface acoustic wave device characteristic properties and sensitivity, *Sensors*, **19** (2019), 1749. https://doi.org/10.3390/s19081749
8. T. Sun, P. Wang, G. Zhang, Y. Chai, Transient analyses of wave propagations in nonhomogeneous media employing the novel finite element method with the appropriate enrichment function, *Comput. Math. Appl.*, **129** (2023), 90–112. https://doi.org/10.1016/j.camwa.2022.10.004
9. L. Chen, H. Lian, S. Natarajan, W. Zhao, X. Chen, S. Bordas, Multi-frequency acoustic topology optimization of sound-absorption materials with isogeometric boundary element methods accelerated by frequency-decoupling and model order reduction techniques, *Comput. Meth. Appl. Mech. Eng.*, **395** (2022), 114997. https://doi.org/10.1016/j.cma.2022.114997
10. L. Chen, H. Lian, Y. Xu, S. Li, Z. Liu, E. Atroshchenko, et al., Generalized isogeometric boundary element method for uncertainty analysis of time-harmonic wave propagation in infinite domains, *Appl. Math. Model.*, **114** (2023), 360–378. https://doi.org/10.1016/j.apm.2022.09.030
11. L. Chen, J. Zhao, H. Lian, B. Yu, E. Atroshchenko, P. Li, A BEM broadband topology optimization strategy based on Taylor expansion and SOAR method-Application to 2D acoustic scattering problems, *Int. J. Numer. Methods Eng.*, 2023. https://doi.org/10.1002/nme.7345
12. S. Zhao, Y. Gu, A localized Fourier collocation method for solving high-order partial differential equations, *Appl. Math. Lett.*, **141** (2023), 108615. https://doi.org/10.1016/j.aml.2023.108615
13. L. Qiu, F. Wang, Y. Gu, Q. H. Qin, Modified space-time radial basis function collocation method for long-time simulation of transient heat conduction in 3D anisotropic composite materials, *Int. J. Numer. Methods Eng.*, **124** (2023), 4639–4658. https://doi.org/10.1002/nme.7327
14. L. Sun, Z. Fu, Z. Chen, A localized collocation solver based on fundamental solutions for 3D time harmonic elastic wave propagation analysis, *Appl. Math. Comput.*, **439** (2023), 127600. https://doi.org/10.1016/j.amc.2022.127600
15. L. Qiu, X. Ma, Q. H. Qin, A novel meshfree method based on spatio-temporal homogenization functions for one-dimensional fourth-order fractional diffusion-wave equations, *Appl. Math. Lett.*, **142** (2023), 108657. https://doi.org/10.1016/j.aml.2023.108657
16. B. Ju, W. Qu, Three-dimensional application of the meshless generalized finite difference method for solving the extended Fisher-Kolmogorov equation, *Appl. Math. Lett.*, **136** (2023), 108458. https://doi.org/10.1016/j.aml.2022.108458

17. S. Jiang, Y. Gu, M. V. Golub, An efficient meshless method for bimaterial interface cracks in 2D thin-layered coating structures, *Appl. Math. Lett.*, **131** (2022), 108080. https://doi.org/10.1016/j.aml.2022.108080
18. Y. Li, C. Liu, W. Li, Y. Chai, Numerical investigation of the element-free Galerkin method (EFGM) with appropriate temporal discretization techniques for transient wave propagation problems, *Appl. Math. Comput.*, **442** (2023), 127755. https://doi.org/10.1016/j.amc.2022.127755
19. P. Bouillard, S. Suleaub, Element-Free Galerkin solutions for Helmholtz problems: fomulation and numerical assessment of the pollution effect, *Comput. Meth. Appl. Mech. Eng.*, **162** (1998), 317–335. https://doi.org/10.1016/S0045-7825(97)00350-2
20. D. Soares Jr, An iterative time-domain algorithm for acoustic-elastodynamic coupled analysis considering meshless local Petrov-Galerkin formulations, *Comput. Model. Eng. Sci.*, **54** (2009), 201–222. https://doi.org/10.3970/cmes.2009.054.201
21. M. Gorakifard, C. Salueña, I. Cuesta, E. Kian Far, The meshless local Petrov-Galerkin cumulant lattice Boltzmann method: Strengths and weaknesses in aeroacoustic analysis, *Acta Mech.*, **233** (2022), 1467–1483. https://doi.org/10.1007/s00707-022-03177-8
22. Y. Gu, J. Lin, C. M. Fan, Electroelastic analysis of two-dimensional piezoelectric structures by the localized method of fundamental solutions, *Adv. Appl. Math. Mech.*, **15** (2023), 880–900. https://doi.org/10.4208/aamm.OA-2021-0223
23. M. H. Gfrerer, M. Schanz, A coupled FEM-MFS method for the vibro-acoustic simulation of laminated poro-elastic shells, *Int. J. Numer. Methods Eng.*, **121** (2020), 4235–4267. https://doi.org/10.1002/nme.6391
24. F. Wang, Y. Gu, W. Qu, C. Zhang, Localized boundary knot method and its application to large-scale acoustic problems, *Comput. Meth. Appl. Mech. Eng.*, **361** (2020), 112729. https://doi.org/10.1016/j.cma.2019.112729
25. Y. Hon, W. Chen, Boundary knot method for 2D and 3D Helmholtz and convection-diffusion problems under complicated geometry, *Int. J. Numer. Methods Eng.*, **56** (2003), 1931–1948. https://doi.org/10.1002/nme.642
26. S. Cheng, F. Wang, G. Wu, C. Zhang, A semi-analytical and boundary-type meshless method with adjoint variable formulation for acoustic design sensitivity analysis, *Appl. Math. Lett.*, **131** (2022), 108068. https://doi.org/10.1016/j.aml.2022.108068
27. X. Wei, W. Luo, 2.5 D singular boundary method for acoustic wave propagation, *Appl. Math. Lett.*, **112** (2021), 106760. https://doi.org/10.1016/j.aml.2020.106760
28. W. Chen, Singular boundary method: A novel, simple, meshfree, boundary collocation numerical method, *Chinese J. Solid Mech.*, **30** (2009), 592–599. https://doi.org/10.19636/j.cnki.cjsm42-1250/o3.2009.06.011
29. X. Wei, C. Rao, S. Chen, W. Luo, Numerical simulation of anti-plane wave propagation in heterogeneous media, *Appl. Math. Lett.*, **135** (2023), 108436. https://doi.org/10.1016/j.aml.2022.108436
30. Z. J. Fu, W. Chen, Y. Gu, Burton-Miller-type singular boundary method for acoustic radiation and scattering, *J. Sound Vibr.*, **333** (2014), 3776–3793. https://doi.org/10.1016/j.jsv.2014.04.025
31. J. White, J. Phillips, T. Korsmeyer, Comparing precorrected-FFT and fast multipole algorithms for solving three-dimensional potential integral equations, In: *Colorado conference on iterative methods*, 1994.

32. Y. S. Smyrlis, A. Karageorghis, A matrix decomposition MFS algorithm for axisymmetric potential problems, *Eng. Anal. Bound. Elem.*, **28** (2004), 463–474. https://doi.org/10.1016/S0955-7997(03)00100-0
33. J. Tausch, J. White, Wavelet-like bases for integral equations on surfaces with complex geometry, *IMACS Ser. Comput. Appl. Math.*, **4** (1998), 251–256.
34. J. R. Phillips, J. K. White, A precorrected-FFT method for electrostatic analysis of complicated 3-D structures, *IEEE Trans. Comput. Aided Des. Integr. Circuits Syst.*, **16** (1997), 1059–1072. https://doi.org/10.1109/43.662670
35. J. R. Phillips, *Rapid solution of potential integral equations in complicated 3-dimensional geometries*, Massachusetts Institute of Technology, 1997.
36. L. Greengard, *The rapid evaluation of potential fields in particle systems*, Cambridge: MIT Press, 1988. https://doi.org/10.1016/0378-4754(88)90063-8
37. W. Hackbusch, B. N. Khoromskij, A sparse H-matrix arithmetic: general complexity estimates, *J. Comput. Appl. Math.*, **125** (2000), 479–501. https://doi.org/10.1016/S0377-0427(00)00486-6
38. W. Hackbusch, B. N. Khoromskij, A sparse $\mathscr{H}$-matrix arithmetic. Part II: Application to multi-dimensional problems, *Computing*, **64** (2000), 21–47. https://doi.org/10.1007/PL00021408
39. M. Bebendorf, Approximation of boundary element matrices, *Numer. Math.*, **86** (2000), 565–589. https://doi.org/10.1007/PL00005410
40. M. Bebendorf, S. Rjasanow, Adaptive low-rank approximation of collocation matrices, *Computing*, **70** (2003), 1–24. https://doi.org/10.1007/s00607-002-1469-6
41. C. Zheng, T. Matsumoto, T. Takahashi, H. Chen, Explicit evaluation of hypersingular boundary integral equations for acoustic sensitivity analysis based on direct differentiation method, *Eng. Anal. Bound. Elem.*, **35** (2011), 1225–1235. https://doi.org/10.1016/j.enganabound.2011.05.004
42. J. Li, W. Chen, Z. Fu, L. Sun, Explicit empirical formula evaluating original intensity factors of singular boundary method for potential and Helmholtz problems, *Eng. Anal. Bound. Elem.*, **73** (2016), 161–169. https://doi.org/10.1016/j.enganabound.2016.10.003
43. S. Cheng, F. Wang, P. W. Li, W. Qu, Singular boundary method for 2D and 3D acoustic design sensitivity analysis, *Comput. Math. Appl.*, **119** (2022), 371–386. https://doi.org/10.1016/j.camwa.2022.06.009
44. L. Godinho, D. Soares Jr, P. Santos, Efficient analysis of sound propagation in sonic crystals using an ACA-MFS approach, *Eng. Anal. Bound. Elem.*, **69** (2016), 72–85. https://doi.org/10.1016/j.enganabound.2016.05.001
45. L. Godinho, P. Amado-Mendes, A. Pereira, D. Soares Jr, An efficient MFS formulation for the analysis of acoustic scattering by periodic structures, *J. Theor. Comput. Acoust.*, **26** (2018), 1850003. https://doi.org/10.1142/S2591728518500032
46. X. Wei, B. Chen, S. Chen, S. Yin, An ACA-SBM for some 2D steady-state heat conduction problems, *Eng. Anal. Bound. Elem.*, **71** (2016), 101–111. https://doi.org/10.1016/j.enganabound.2016.07.012

AIMS Press